Cogn Neurodyn (2013) 7:197–212
DOI 10.1007/s11571-012-9226-9

RESEARCH ARTICLE

# Bursting synchronization dynamics of pancreatic $\beta$-cells with electrical and chemical coupling

**Pan Meng · Qingyun Wang · Qishao Lu**

Received: 25 March 2012 / Revised: 17 September 2012 / Accepted: 11 October 2012 / Published online: 25 October 2012


**Abstract** Based on bifurcation analysis, the synchronization behaviors of two identical pancreatic $\beta$-cells connected by electrical and chemical coupling are investigated, respectively. Various firing patterns are produced in coupled cells when a single cell exhibits tonic spiking or square-wave bursting individually, irrespectively of what the cells are connected by electrical or chemical coupling. On the one hand, cells can burst synchronously for both weak electrical and chemical coupling when an isolated cell exhibits tonic spiking itself. In particular, for electrically coupled cells, under the variation of the coupling strength there exist complex transition processes of synchronous firing patterns such as "fold/limit cycle" type of bursting, then anti-phase continuous spiking, followed by the "fold/torus" type of bursting, and finally in-phase tonic spiking. On the other hand, it is shown that when the individual cell exhibits square-wave bursting, suitable coupling strength can make the electrically coupled system generate "fold/Hopf" bursting via "fold/fold" hysteresis loop; whereas, the chemically coupled cells generate "fold/subHopf" bursting. Especially, chemically coupled bursters can exhibit inverse period-adding bursting sequence. Fast–slow dynamics analysis is applied to explore the generation mechanism of these bursting oscillations. The above analysis of bursting types and the transition may provide us with better insight into understanding the role of coupling in the dynamic behaviors of pancreatic $\beta$-cells.

**Keywords** Coupled cells · Bursting · Continuous spiking · Bifurcation · Fast–slow dynamics analysis

P. Meng
School of Basic Courses, Guangdong Pharmaceutical University, Guangdong 510006, China

Q. Wang (✉) · Q. Lu
Department of Dynamics and Control, Beihang University, Beijing 100191, China
e-mail: nmqingyun@163.com

## Introduction

Pancreatic $\beta$-cells located in islets of Langerhans in the pancreas are responsible for the synthesis and secretion of insulin in response to a glucose challenge. Like nerve and endocrine cells, pancreatic $\beta$-cells are electrically excitable (Ashcroft and Rorsman 1989) and the electrical firing patterns typically come in the form of bursting, characterized by an active phase of fast spiking followed by a quiescent phase without spiking (Dean and Mathews 1970). It is well-known that bursting can be exhibited by a wide range of nerve and endocrine cells, and it is likely one of the most important and distinctive patterns in dynamic behaviors. Bursting activity is also important for pancreatic $\beta$-cells because it leads to oscillations in the intracellular free $Ca^{2+}$ concentration, which in turn leads to oscillations in insulin secretion (Ravier et al. 1999).

There is strong evidence that impaired insulin secretion is the initial and main genetic factor predisposing to Type II diabetes (Bergsten 2000). Insulin secretion is a complex multicellular process, which depends on interactions between $\beta$-cells within an islet as well as on the interactions between islets in the pancreas (Krasimira et al. 2006). In order to observe an overall oscillatory insulin profile, it is necessary to understand the collective behavior of $\beta$-cells. Eelectrical coupling through gap junctions and chemical coupling through chemical synapse have been suggested to be exists in regulating basal insulin release

(Calabrese et al. 2000; Rorsman et al. 1989; Salehi et al. 2005). Evidence for electrical coupling via gap junctions between islet cells has previously been provided by electron microscopy, recordings of membrane potential and currents using sharp intracellular electrodes (Zhang et al. 2008; Orci et al. 1975; Meissner 1976).

Synchronization, as an emerging phenomenon of a population of dynamically interacting units (Arenas et al. 2008; Wang and Jiao 2006; Wang and Zhang 2003; Zhang et al. 2010), has been extensively studied both in coupled cells (Wang et al. 2011;Marek and Stuchl 1975) or complex networks (Gomez-Gardenes et al. 2007; Volman et al. 2011; Sun et al. 2011). It has been demonstrated that the electrical activity of two electrically coupled $\beta$-cells can exhibit different forms of synchronous activities, both in vivo (Valdeolmillos et al. 1996) and in vitro (Eddlestone et al. 1984). Numerical simulations have been used to examine the role of the electrical coupling strength in synchronous behaviors within intact islets. Based on a minimal but representative model of bursting electrical activity in the pancreatic $\beta$-cell, Sherman and Rinzel considered an idealized case of pairs of identical cells, and showed that they can be converted from tonic spiking to bursting by weak electrical coupling (Sherman and Rinzel 1991, 1992). Later, Sherman further gave the bifurcation analysis of a coupled pair of identical bursters by extending the theory of bursting for square-wave bursters from single cell to coupled cells (Sherman 1994). Using the same method, the normal form analysis of coupled bursters was primarily presented in (De Vries and Sherman 1998). The importance of the bifurcation structure for the synchronization of coupled cells has also been studied in (Perc and Marhl 2004a, b).

Although the minimal model explains the minimum conditions needed for generating bursting oscillations, it doesn't involve the ATP-sensitive $K^+$ current. Given that this ionic current does exist and plays an important role in pancreatic $\beta$-cells, the minimal model was extended by including the ATP-sensitive $K^+$ current to get the modified model, proposed by De Vries and Sherman (2000). In this paper, it was shown that weak electrical coupling can still induce synchronous bursting oscillations in cells,which are incapable of bursting individually, and the coupled system will return to the in-phase (IP) spiking state eventually under strong electrical coupling. However, how the synchronous bursting changes during the transition process is still not clear. Here we show that under moderate electrical coupling strength, two regular firing patterns can be produced in the intermediate process, that is, the anti-phase (AP) spiking firing pattern and another completely different bursting synchrony, respectively. We also show that weak electrical coupling can make the two-coupled cells transit to burst synchronization with "fold/Hopf" bursting via the "fold/fold" hysteresis loop while the isolated single cell only exhibits "fold/homoclinic" type of bursting.

As mentioned above, electrical coupling has been well studied in the pancreatic islets, and is believed to account for signal synchronization of islet cells; in contrast, the influence of chemical coupling on islet synchronization and its physiological response are less concerned. It was known that neurons communicate through synapses more often than gap junctions and neuronal network with chemical coupling can be successful in producing important biological rhythms (Rubin and Terman 2002). Chemical coupling also exists in pancreatic $\beta$-cells. The existence of diffusible chemical coupling in pancreatic $\beta$-cells has been presented in that changes in the flow rate appear due to the period of oscillation of cells (Cunningham et al. 1996; Kennedy et al. 2002). Here, we investigate the effects of chemical coupling on the two chemically coupled $\beta$-cells. In particular, when the single cell exhibits continuous spiking, the chemically coupled system can exhibit burst synchronization, and the bursting types of which are similar to the electrical coupling case. However, the bifurcation mechanism is totally different. In addition, when the single cell exhibits "fold/homoclinic" type of bursting, the coupled system generates the inverse period-adding bursting sequence in a certain range of the coupling strength. Moreover, with strong chemical coupling strength, the two-cell model can generate complete burst synchronization with "fold/subHopf" type of bursting.

This paper is organized as follows. In "Dynamics of electrically coupled cells" and "Dynamics of chemically coupled cells", we show how the coupling strength affects the synchronization firing behaviors of two coupled $\beta$-cells connected by electrical and chemical couplings, respectively. "Conclusion" deals with a discussion of the results. In the "Appendix", we include the isolated single model and a description for the generation mechanism of continuous spiking and the "fold/homoclinic" bursting of the individual cell.

## Dynamics of electrically coupled cells

The main goal of the paper is to analyze what will happen in synchronization behaviors of the coupled pancreatic $\beta$-cells when an individual cell exhibits either tonic spiking or "fold/homoclinic" bursting, which is shown in the "Appendix". In order to well understand the effects of coupling strength on the dynamics of the coupled system, fast–slow dynamics analysis is extended to a pair of coupled identical cells. The results are presented in "Dynamics of electrically coupled cells" and "Dynamics of chemically coupled cells" according to the types of electrical and chemical coupling, respectively. Each section will be

**Table 1** Parameter values

| | | | | |
|---|---|---|---|---|
| $g_{Ca} = 3.6$ | $v_{Ca} = 20$ mV | $v_m = -20$ mV | $\theta_m = 12$ mV | $\tau = 20$ ms |
| $g_K = 10$ | $v_K = -75$ mV | $v_n = -17$ mV | $\theta_n = 5.6$ mV | $\lambda = 0.8$ |
| $g_{K(ATP)} = 1.2$ | $p = 0.5$ | $v_s = -22$ mV | $\theta_s = 8$ mV | $\tau_s = 20{,}000$ ms |
| $g_s = 2$ or 4 | | | | |

divided into two subsections depending on the dynamical behavior of the individual cell.

To incorporate the electrical coupling of two identical pancreatic $\beta$-cells via gap junctions, the variables $v$, $n$ and $s$ are indexed by the cell number and a coupling term is added to the first equation as follows:

$$\tau \frac{dv_i}{dt} = -I_{Ca}(v_i) - I_k(v_i, n_i) - I_s(v_i, s_i) - I_{K(ATP)}(v_i, p_i) - g_c(v_i - v_j) \quad (1)$$

$$\tau \frac{dn_i}{dt} = \lambda[n_\infty(v_i) - n_i] \quad (2)$$

$$\tau_s \frac{ds_i}{dt} = s_\infty(v_i) - s_i \quad (3)$$

where $g_c(v_i - v_j)$ represents the coupling term, and $g_c$ is the coupling strength independent of $v_1$ and $v_2$. The values of fixed parameters used in this paper are listed in Table 1.

## Two coupled spiking cells

When $g_s = 2$, the single cell exhibits continuous spiking (see Fig. 14a in the "Appendix"). It is pointed out that weak electrical coupling can induce synchronous bursting oscillations in coupled cells that are incapable of bursting alone. The strong coupling can make the cells revert to spiking again (De Vries and Sherman 2000), which also can be seen clearly from Fig. 1, where the bifurcation diagram of ISIs versus $g_c$ is illustrated.

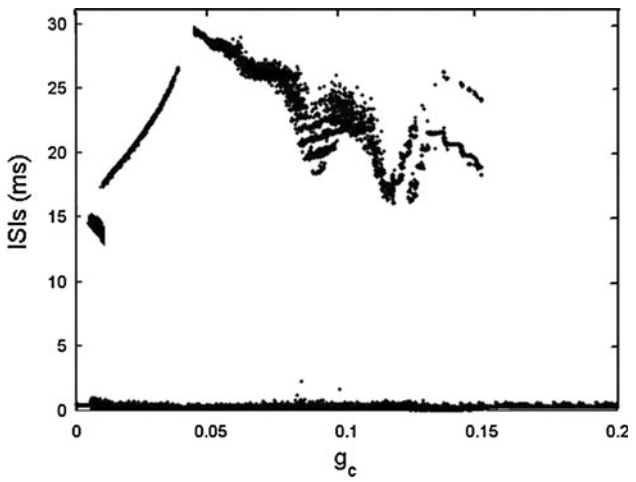


**Fig. 1** Bifurcation *diagram* of ISIs versus the electrical coupling strength $g_c$ in the two electrically coupled cells

Here we can find that between the two extreme cases, there exist other synchronous activities during the transition process. If only regular firing patterns are concerned, it can be seen that with $g_c$ increasing, the continuous spiking transits to regular bursting firstly, and then experiences spiking in a certain range of $g_c$. Soon afterwards, the coupled system transits to bursting again, and if the coupling strength is strong enough, it finally returns to spiking again. Four typical cases of the electrical coupling strengths are chosen as representatives to understand the whole transition process.

### *The case of $g_c = 0.01$*

Now the two-cell model generates synchronous bursting (see Fig. 2), and the spikes within burst are anti-phase (see Fig. 3a). The two-coupled cells achieving bursting synchronization have $s_1 \approx s_2$ for the slow variable. In order to study the bifurcation structure for the fast subsystem of the coupled system, that is, Eqs. (1), (2), we can treat $s_1$ (or $s_2$) as the bifurcation parameter (Sherman and Rinzel 1991, 1992; Sherman 1994; Sherman et al. 1988; De Vries and Sherman 2000; Perc and Marhl 2004a, b). Owing to the fact of achieving synchronization in the coupled system, there must exist some function relation between $v_1$ and $v_2$. Hence, we can only choose $v_1$ (or $v_2$) as the state variable of the synchronously coupled cells.

The bifurcation of the fast subsystem with respect to the slow variable $s_1$ is presented in Fig. 3b. For clarity, only the pertinent solution branches are included. It is seen that the steady state is the same as that in the single cell. But, on the upper branch there are two supHopf bifurcations instead of only one. The periodic branch originated from the left Hopf bifurcation point H1, corresponding to the synchronous IP bursting solutions (marked by red color in figures) of the coupled system, is detected at the same parameter value as that of the single cell. The IP branch is initially stable, but loses stability via the pitchfork of periodic bifurcation (BP). A branch of synchronized AP bursting solutions (marked by blue color in figures) emerges from the second supHopf bifurcation H2. It is unstable initially, but becomes stable via the torus bifurcation (TR) up to the fold limit cycle bifurcation (LC). Moreover, AP has smaller amplitude than IP, as a result, the termination of the AP branch lies to the right of that of the IP branch. Thus there exists bistability between the steady state on the lower branch of the $Z$ shaped curve and

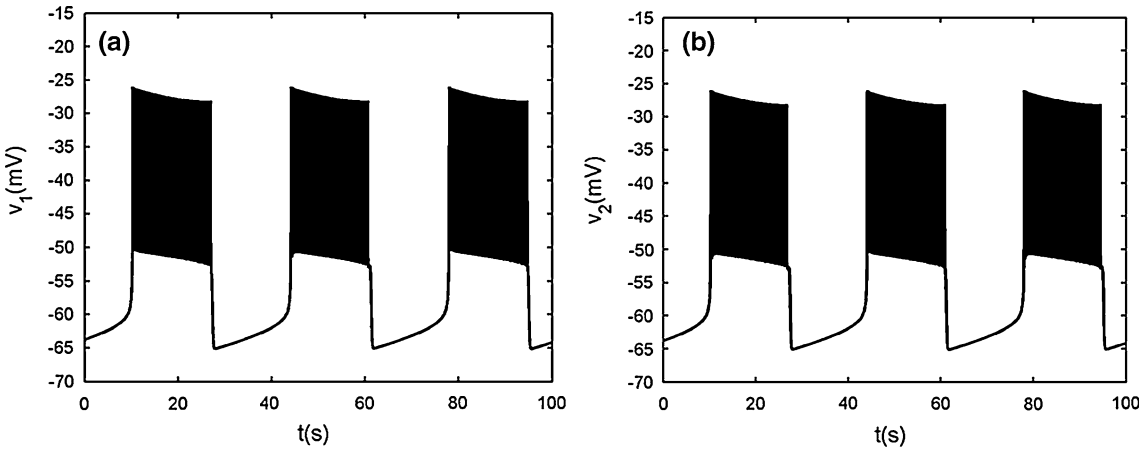


**Fig. 2** Two electrically coupled cells with $g_s = 2$, $g_c = 0.01$. **a** Time series of the variable $v_1$. **b** Time series of the variable $v_2$

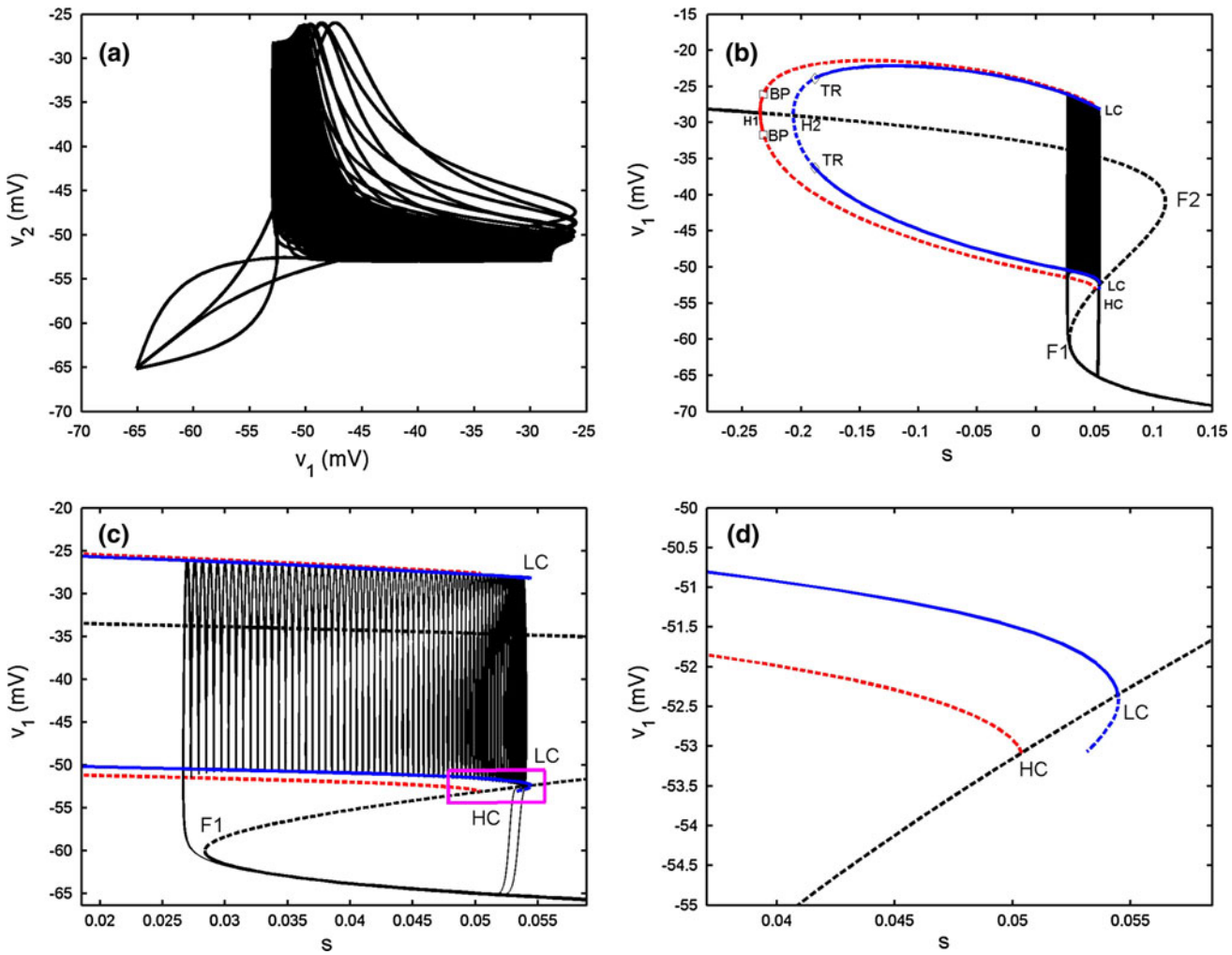


**Fig. 3** Two electrically coupled cells with $g_s = 2$, $g_c = 0.01$. **a** The projection of the coupled system on ($v_1$, $v_2$) plane. **b** Bifurcation *diagram* for the fast subsystem of two-cell model [Eqs. (1), (2)] with $s = s_1 = s_2$ taken as the bifurcation parameter. H1 and H2 refer to the supHopf bifurcations, BP refers to the pitchfork of periodic bifurcations labeled by *open squares*, TR refers the torus bifurcation labeled by *diamonds*, F1 and F2 refer to the fold bifurcations, HC refers to the homoclinic bifurcation, LC refers to the fold limit cycle bifurcation. The *red and blue lines* represent IP and AP branches, respectively. **c** The enlargement of the bistability region in **b**. The phase *plot* of the whole system is also included. **d** The magnification of the *rectangular area* in **c**. (Color figure online)

the periodic AP solution on the AP branch, which gives rise to the bursting oscillation.

In order to better understand the bursting pattern, we start to explain the system behavior at the silent phase of bursting. It is seen that the trajectory moves left along the lower branch of the $Z$ shaped curve until it meets the fold bifurcation F1. Then the system enters the active phase without the supHopf bifurcation H1 participated in the trajectory and there is no IP solution. Instead, the trajectory mainly lingers on the AP branch during the active phase, which indicates that the two cells are AP synchronized. The active phase of trajectory ends with the fold LC, where the stable periodic solution becomes unstable (see Fig. 3d), and then the trajectory returns to the bottom branch, restarting the cycle. According to the classification scheme of bursting mechanisms given in (Izhikevich 2000), this type of bursting belongs to the "fold/fold limit cycle" bursting. It marks the beginning of the complex transition process.

*The case of $g_c = 0.04$*

In this case, the synchronization of AP continuous spiking is shown in Fig. 4a, b. It is clearly observed that the amplitude of spiking becomes smaller than that of individual cell (see Fig. 14a in the "Appendix"). Fast–slow dynamics analysis is applied to explore the dynamical behavior of this phenomenon as shown in Fig. 4c. Compared with Fig. 3b, the $Z$shaped curve persists with the left supHopf bifurcation H1 being unchanged, and the IP branch also ends with the homoclinic bifurcation HC. However, now the upper branch of the $Z$ shaped curve has three supHopf bifurcation points together, that is, H1 at $s = -0.235$, H2 at $s = -0.1183$ and H3 at $s = 0.1056$,

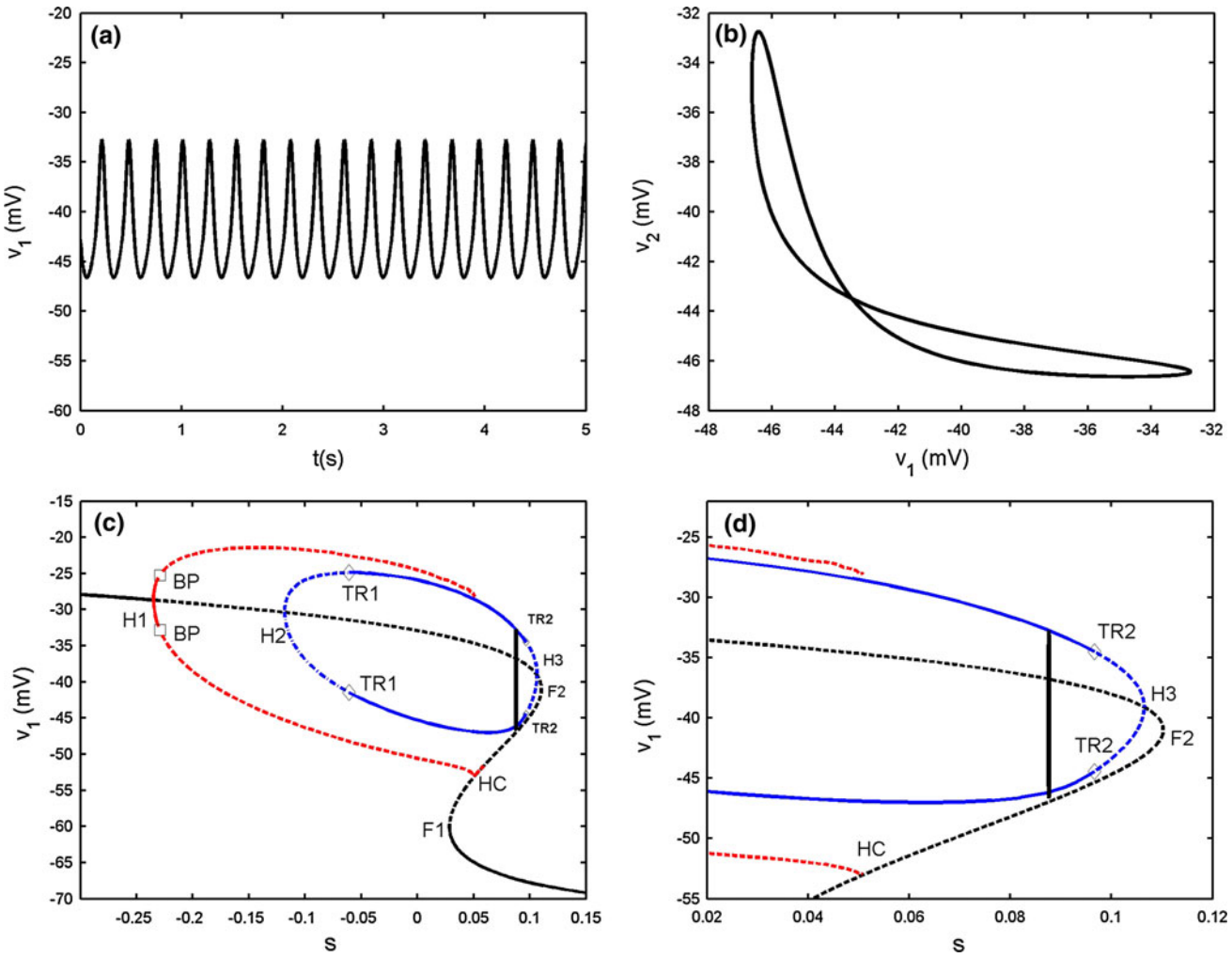


**Fig. 4** Two electrically coupled cells with $g_s = 2$, $g_c = 0.04$. **a** Time series of the variable $v_1$. **b** The projection on ($v_1$, $v_2$) plane. **c** Fast–slow dynamics analysis of the fast subsystem. H1, H2 and H3 refer to the supHopf bifurcations, TR1 and TR2 refer to the torus bifurcations in the AP branch, F1 and F2 refer to the fold bifurcations, HC refers to the homoclinic bifurcation. **d** The magnification of the region near the *right* knee of the $Z$ shaped *curve* in **c**

respectively. Moreover, two periodic branches originating from the points H2 and H3 are connected together to form a closed loop, which is separated from the middle branch and represents the AP branch, as seen in Fig. 4c. In addition, the fast subsystem has extra TRs labeled as TR2 in the right side of AP branch. It is noted that the trajectory locates on the AP branch totally so that the coupled system exhibits AP continuous spiking. It is noticed that the amplitude is very small, only about 10 mv, which is not very practical in a real neural system. It is interesting to explore essence of this phenomenon in the present systems studied in the future.

*The case of* $g_c = 0.0435$

As the first case with $g_c = 0.01$, the electrically coupled system exhibits bursting synchronization with the spikes being AP (see Fig. 5a, b). Compared with Fig. 2, it is seen that the burst period of the variable $v_1$ becomes much bigger with $g_c$ increasing, and at the same time the spike amplitude is decreased. Fast–slow dynamics analysis is illustrated in Fig. 5c. The bifurcation structure of the fast subsystem is very similar to Fig. 4c. Hence, the details about the bifurcation diagram are omitted here. Like the first case, there exists bistability between the stable nodes on the lower branch and the stable AP branch up to the second TR TR2. Moreover, the AP branch, which starts from the second supHopf bifurcation $H_2$ at $s = -0.1089$ and terminates at the third supHopf bifurcation $H_3$ at $s = 0.1054$, is far from the IP branch originating from the left point $H_1$ at $s = -0.235$. Therefore, it can be seen clearly that during the active phase the two cells are synchronized IP at first, and then transit to AP synchronization very quickly. The disappearance of the silent phase and active phase depends on the fold bifurcation F1 and the TR TR2, respectively. Thus, this type of bursting pattern is

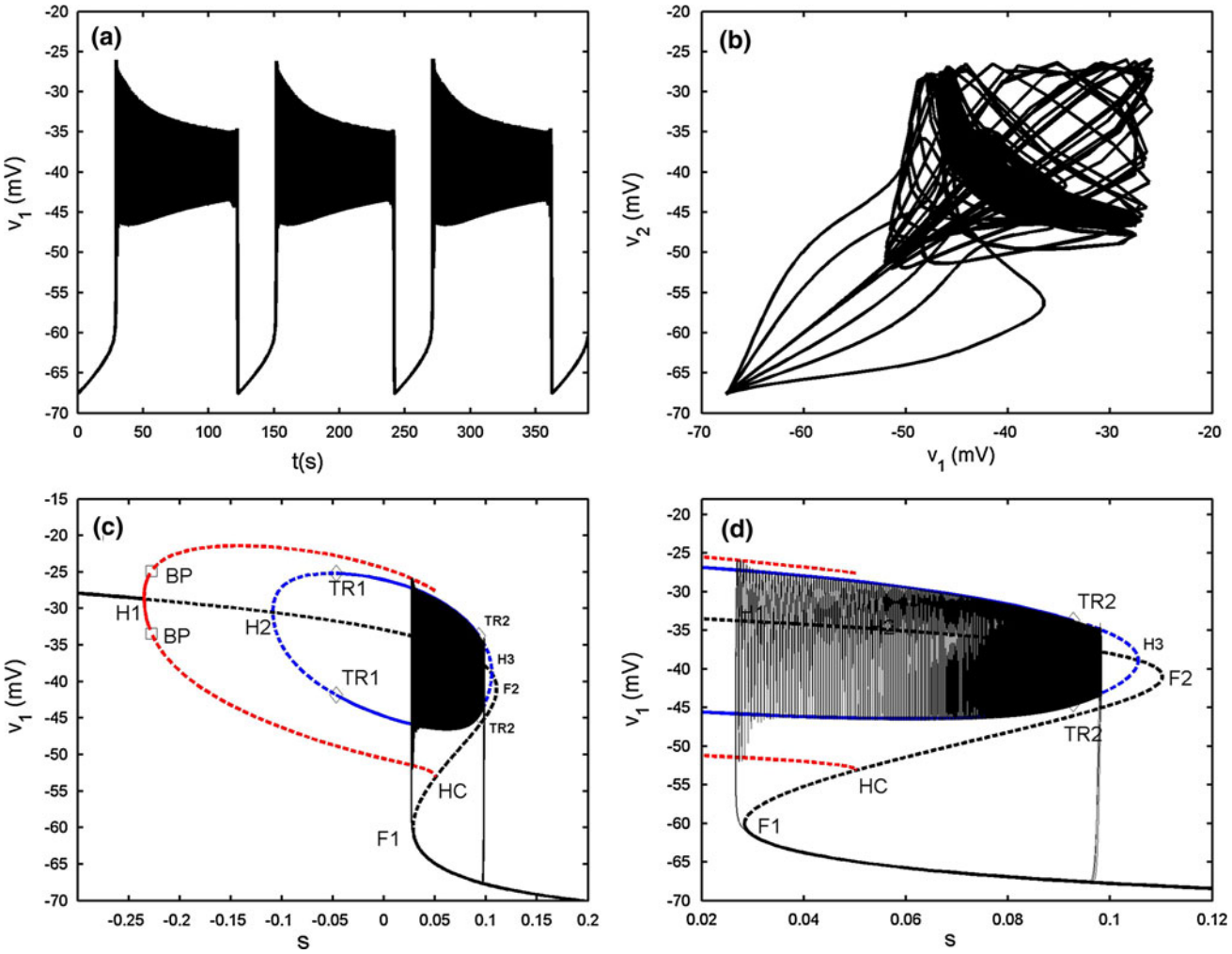


**Fig. 5** Two electrically coupled cells with $g_s = 2$, $g_c = 0.0435$. **a** Time series of the variable $v_1$. **b** The projection on ($v_1$, $v_2$) plane. **c** Fast–slow dynamics analysis of the fast subsystem. The description of the *lines* and *points* is the same as that in Fig. 4c. **d** The magnification of the bistability region in **c**

classified as "fold/torus" type. Compared with previous results, Cases 2 and 3 are new phenomena.

*The case of* $g_c = 0.15$

The two-coupled cells achieve complete spiking synchronization (see Fig. 6a, b). Compared with the former cases, the upper branch of the $Z$ shaped curve has only one sup-Hopf bifurcation H1. Hence, the IP branch only exists while the AP branch disappears. Moreover, there are three pitchforks of BPs on the IP branch, labeled as BP1, BP2 and BP3, respectively. The stable IP branch becomes unstable via the first pitchfork of BP BP1 until the second pitchfork of BP BP2 is reached, and then it is stable and reverts to be unstable again via the third pitchfork of BP BP3. The bifurcations BP2 and BP3 are close together, the local enlargement of the neighborhood near the two points is given in Fig. 6d to distinguish them. It is seen that the spiking solution is totally located in the region between the two bifurcations BP2 and BP3. Thus, the two cells behave identically. It must be pointed out that even though the shape of the bifurcation diagram of the two-coupled cells is almost the same as that of the single cell, and the dynamical behavior of the variable $v_1$ (or $v_2$) is also nearly unchanged as mentioned above. However, the detailed bifurcation structure of the fast subsystem is actually different, especially for the existence of three pitchforks of BPs. This case is the last situation we listed in the paper when two continuous spiking cells are electrically coupled.

At last, we point out that if the coupling strength is larger than the critical value $g_c = 0.2$, the electrically coupled system still produce complete spiking synchronization and the bifurcation structure of the fast subsystem is identical to that of the single cell.

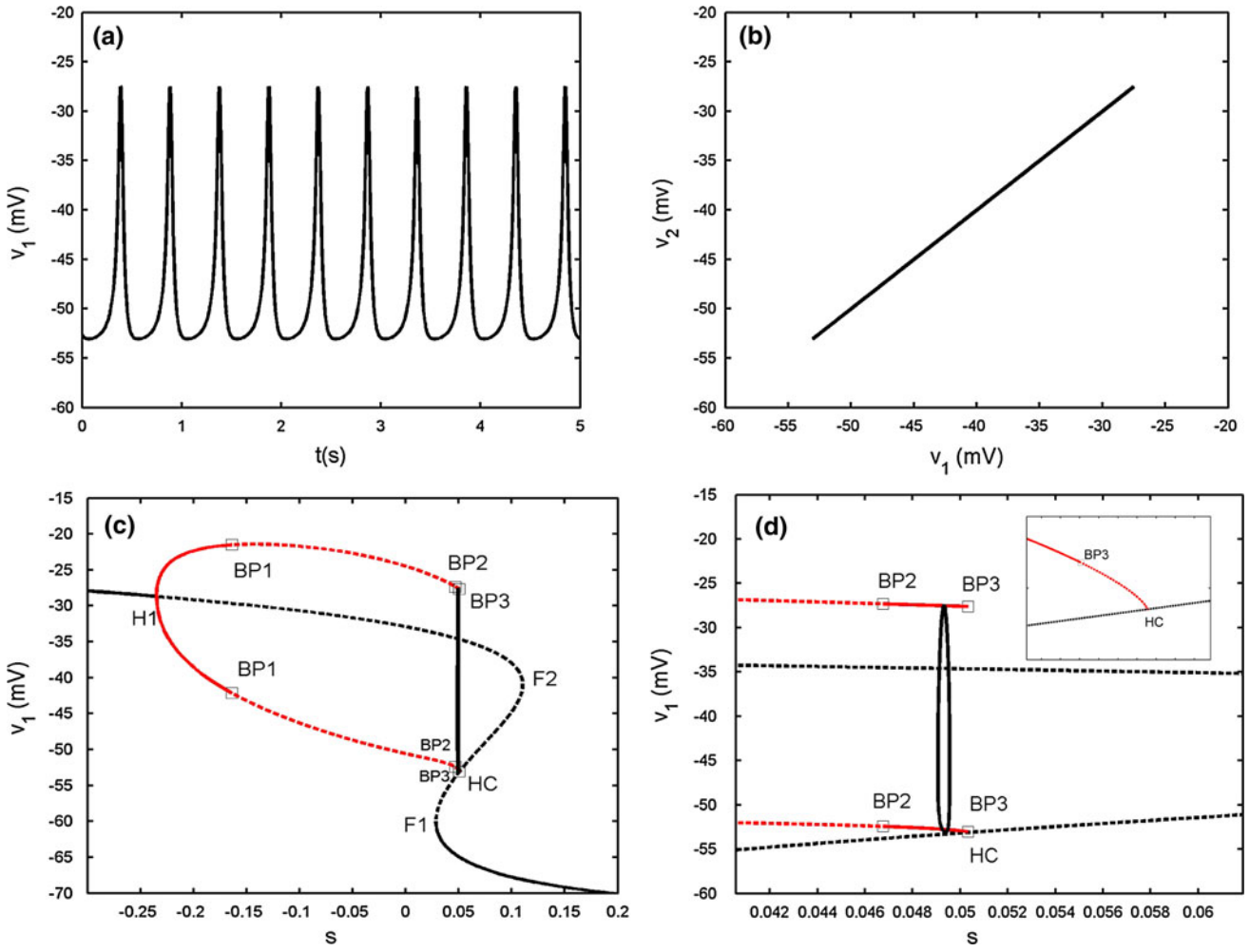


**Fig. 6** Two electrically coupled cells with $g_s = 2$, $g_c = 0.15$. **a** Time series of the variable $v_1$. **b** The projection on ($v_1$, $v_2$) plane. **c** Fast–slow dynamics analysis of the fast subsystem. BP1, BP2 and BP3 refer to the pitchfork of periodic bifurcations. **d** The magnification of the region between the bifurcations BP2 and BP3 in **c**. The *subfigure* in the *right upper* corner is the magnification of the region near the point HC

Two coupled bursters

In the above statement, it is shown that weak electrical coupling can make continuous spiking transit to bursting. Actually, the single system and electrically coupled system with proper coupling strength, both of which can be able to generate bursting on their own, while the generation mechanism for bursting may be different with details described below.

When $g_s = 4$, as illustrated in Fig. 15a in the "Appendix", the isolated single cell exhibits "fold/homoclinic" type of bursting. The two-cell model with the electrical coupling strength $g_c = 0.05$ generates the synchronized bursting, but the spikes are anti-phased (see Fig. 7b). Compared with the original single model, it is observed that weak electrical coupling makes the burst period become longer, about 50 s. The bifurcation diagram is given in Fig. 7c. It is noticed that the bifurcation structure of the fast subsystem for the coupled system is almost the same as that of Fig. 5c. However, the bursting trajectory with the projection on ($v_1$, $s_1$) plane is quite different. During the active phase of bursting, the trajectory has a short stay in oscillating between the maximum and minimum of the IP branches firstly, thus it has some big spikes at the beginning of the active phase. Afterwards it starts to wrap towards the stable periodic branch emerged from the second Hopf bifurcation H2. The trajectory experiences the third Hopf bifurcation H3, and then spirals the stable focus originating from $H_3$ with amplitude decaying as shown in Fig. 7d. Finally, the upper resting state transits to the lower stable branch via the fold bifurcation F2, and initiates the silent phase of bursting. According to the classification of bursting, this type of bursting belongs to the "fold/Hopf" bifurcation via "fold/fold" hysteresis type.

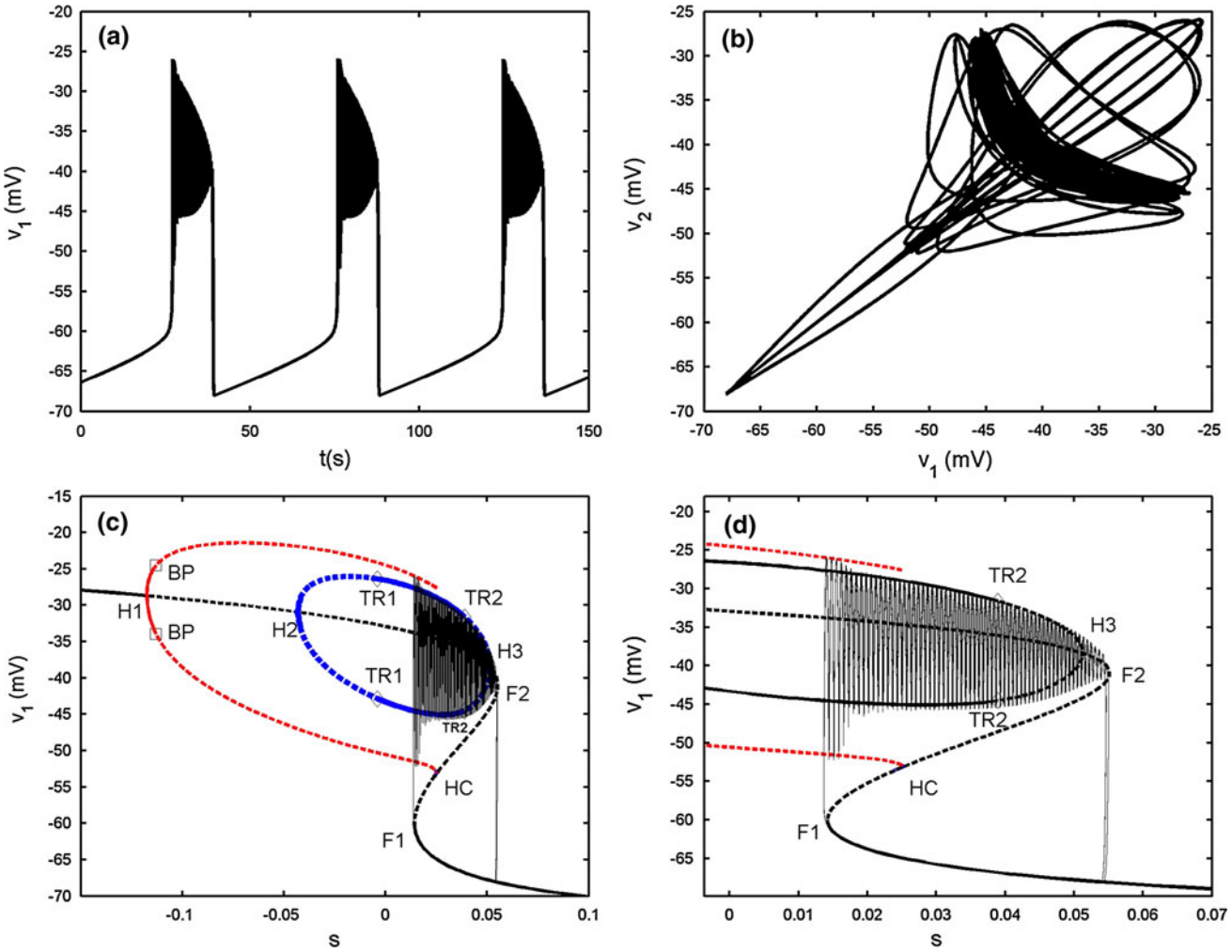


**Fig. 7** Two electrically coupled cells with $g_s = 4$, $g_c = 0.05$. **a** Time series of the variable $v_1$. **b** The projection on ($v_1$, $v_2$) plane. **c** Fast–slow dynamics analysis of the fast subsystem. The description of the *lines* and *points* is the same as that in Fig. 6c. **d** The magnification of the bistability region in **c**

### Dynamics of chemically coupled cells

In this section, we consider two coupled pancreatic $\beta$-cells with chemical synaptic coupling,

$$\tau\frac{dv_{1,2}}{dt} = -I_{Ca}(v_{1,2}) - I_k(v_{1,2}, n_{1,2}) - I_s(v_{1,2}, s_{1,2}) - I_{K(ATP)}(v_{1,2}, p_{1,2}) + \frac{g_{syn}(v_{syn} - v_{1,2})}{1 + \exp(-\sigma(v_{2,1} - \theta))} \quad (4)$$

$$\tau\frac{dn_{1,2}}{dt} = \lambda[\eta_\infty(v_{1,2}) - n_{1,2}] \quad (5)$$

$$\tau_s\frac{ds_{1,2}}{dt} = s_\infty(v_{1,2}) - s_{1,2} \quad (6)$$

where the subscript 1 (or 2) represents cell 1 (or 2), $g_{syn}$ is the synaptic coupling strength, and $v_{syn}$ is the synaptic reversal potential that determines the type of synapses, which is dependent on the type of synaptic transmitter released from a presynaptic cell and its receptors. The coupling becomes excitatory (or inhibitory) for $v_{syn} > v_c$ (or $v_{syn} < v_c$), where $v_c$ is the equilibrium potential for single cell. Here we choose $v_{syn} = -15$ mv, thus the coupling system is on the excitatory regime. $\theta$ is the synaptic threshold, above which the postsynaptic cell can be affected by the presynaptic one, and it is fixed at $-30$ mv; The $\sigma = 10$ represents a constant rate for the onset of excitation. The values of other parameters referred in the equations are the same as the single cell which can be found in Table 1.

#### Two coupled spiking cells

When $g_s = 2$, it is known that the single cell exhibits tonic spiking (see Fig. 14a in the "Appendix"). The purpose of this part is to show that two chemically coupled cells with moderate coupling strength can also generate bursting oscillations but with less cases of firing pattern, compared with the results for electrical coupling in "Two coupled spiking cells".

##### *The case of $g_{syn} = 0.03$*

In such case, the dynamics of the two-coupled cells are bursting synchronization (see Fig. 8) with AP spiking inside bursts (see Fig. 9a). As the cases referred in the electrical coupling, the slow variables $s_1 \approx s_2$ is also available. Thus fast–slow dynamics analysis can also be applied to the chemically coupled system. The fast subsystem is consisted of Eqs. (4), (5) with the slow variable $s = s_1 = s_2$ taken as the bifurcation parameter. It is noticed that the $Z$ shaped curve of the fast subsystem is identical to that of the single cell. Especially, the twofold bifurcations F1 and F2 are detected at the same parameter values as the individual cell.

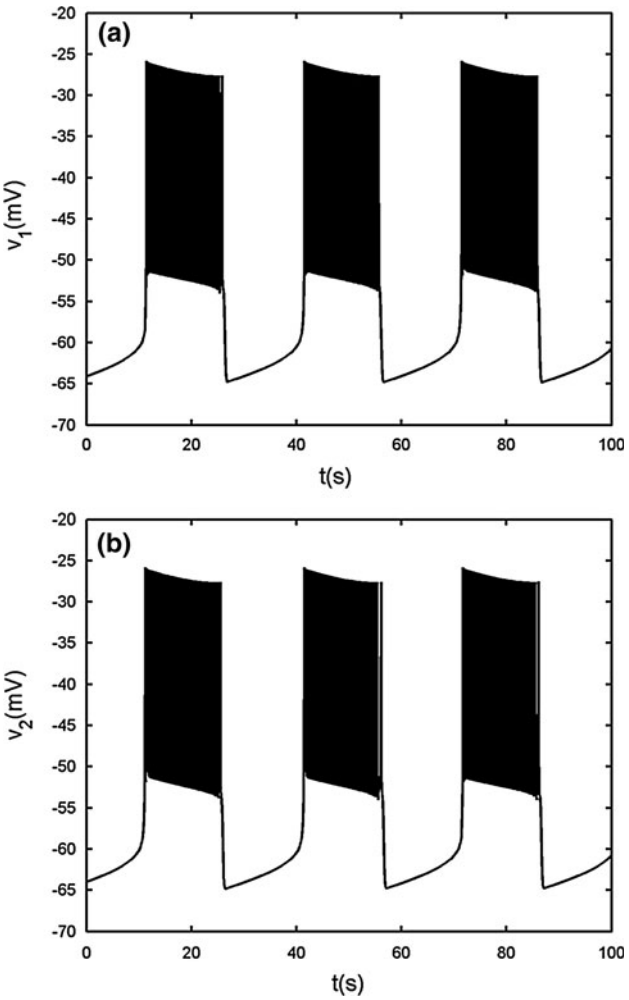


**Fig. 8** Two chemically coupled cells with $g_s = 2$, $g_{syn} = 0.05$. **a** Time series of the variable $v_1$. **b** Time series of the variable $v_2$

Similar to Fig. 3b, the upper branch of the $Z$ shaped curve also has two supHopf bifurcations H1 and H2. However, the left Hopf bifurcation H1 is taken at a different value at $s = -0.1815$, indicating that this is distinct from the electrical coupling cases. The IP branch originating from the H1 point becomes stable via the fold LC LC1 up to the pitchfork of BP. The AP branch emerging from the second Hopf bifurcation H2 changes stability via the TR, while it passes through the fold LC LC2 with the stability unchanged in this process. As $s$ decreases, the silent phase of bursting corresponding to the lower stable branch of the $Z$ shaped curve transits to the spiking state corresponding to the stable limit cycle around the upper branch of the $Z$ shaped curve via the fold bifurcation F1. Then the trajectory starts to wrap towards the stable AP branch, thus within each burst the spikes are completely anti-phased. After a time interval, the AP branch becomes unstable via the fold LC LC3 as shown in Fig. 9d. Hence the trajectory jumps to the lower rest state to complete one loop. In a word, the generation mechanism

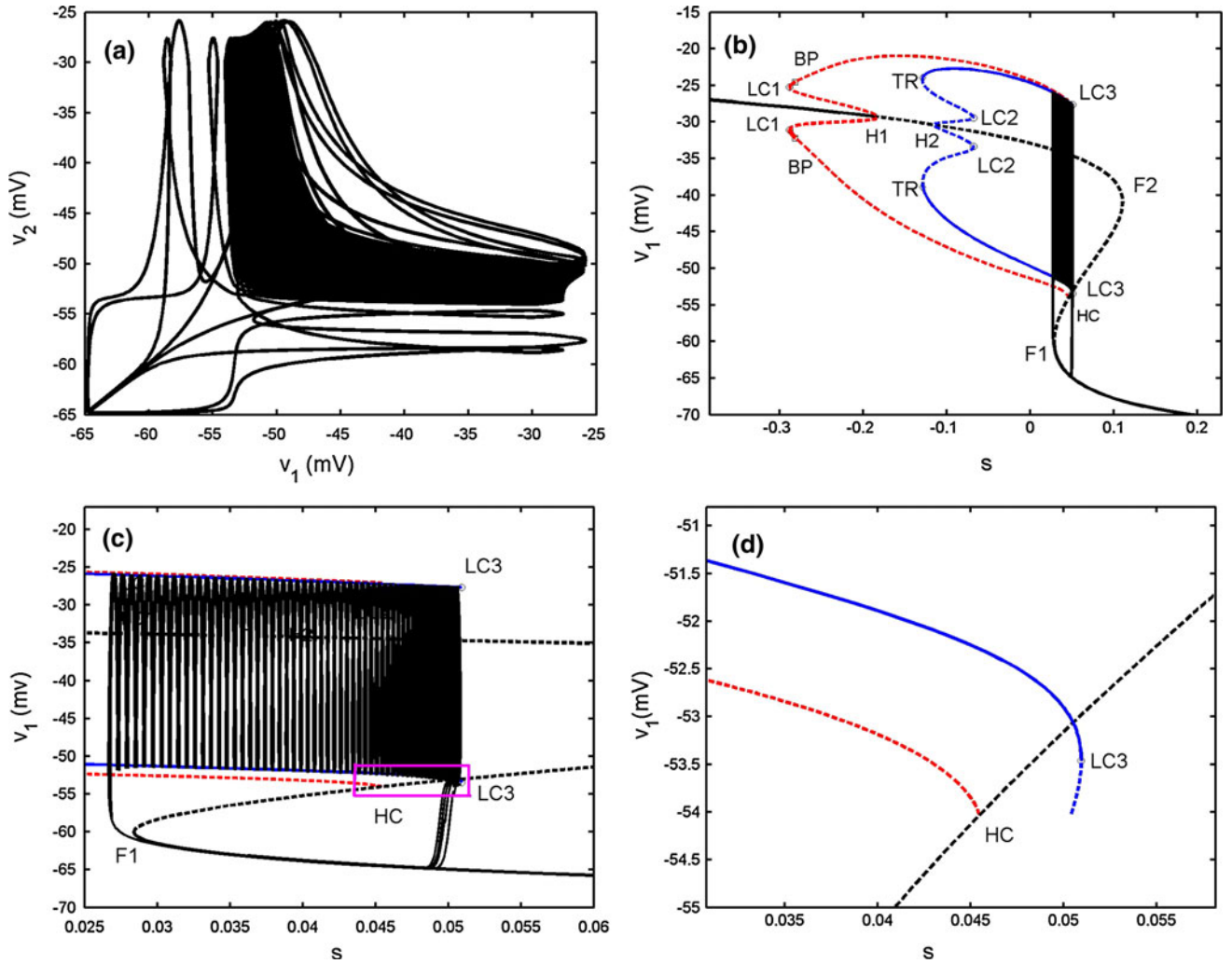


**Fig. 9** Two chemically coupled cells with $g_s = 2$, $g_{syn} = 0.05$. **a** The projection on ($v_1$, $v_2$) plane. **b** Bifurcation *diagram* for the fast subsystem of two-cell model [Eqs. (4), (5)] with $s = s_1 = s_2$ taken as the bifurcation parameter. LC1, LC2 and LC3 refer to the fold limit cycle bifurcations, respectively. The description of the *lines* and other *points* is the same as that in Fig. 3b. **c** The enlargement of the bistability region in **b**. **d** The magnification of the *rectangular area* in **c**

of this type of bursting is similar to that of Fig. 3b. This bursting also belongs to the "fold/fold limit cycle" type; whereas the bifurcation structure of the fast subsystem is very different.

*The case of* $g_{syn} = 0.13$

With this coupling strength, the coupled system is still in bursting synchronization. Thus, it experiences different firing patterns (see Fig. 10a) due to the changes of the AP branch. In Fig. 10c, the unstable AP branch emerged from the second Hopf bifurcation H2 at $s = -0.1081$ becomes stable directly via the TR without the participation of the fold LC as that in Fig. 9b. Moreover, the AP branch is still unstable when the trajectory jumps to the upper branch via the fold bifurcation F1. Hence, the trajectory oscillates along the IP branch at the beginning, which causes the early stage of the active phase. As time is evolving, the trajectory is attracted by the stable limit cycle that results from the TR. Thereby, the AP synchronization starts until the fold LC LC2 is reached. Hence, compared with Fig. 8, this type of bursting can also be classified as "fold/fold limit cycle" type, while the firing pattern has some difference.

Two coupled bursters

When $g_s = 4$, the single cell produces square-wave bursting (see Fig. 15a in the "Appendix"). The bifurcation structure of ISIs of two chemically coupled pancreatic $\beta$-cells is given in Fig. 11, in which the chemical coupling

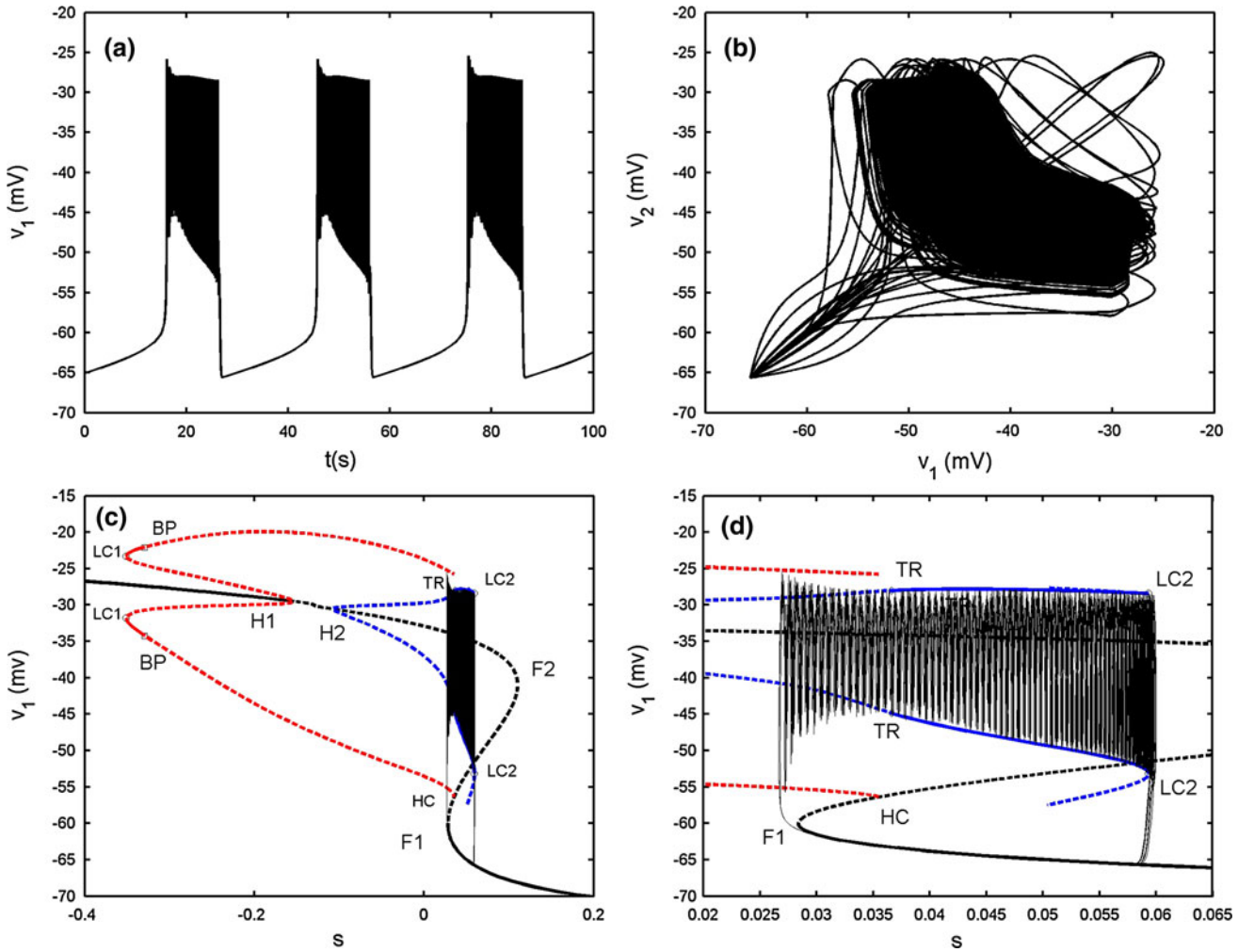


**Fig. 10** Two chemically coupled cells with $g_s = 2$, $g_{syn} = 0.13$. **a** Time series of the variable $v_1$. **b** The projection on ($v_1$, $v_2$) plane. **c** Fast–slow dynamics analysis of the chemically coupled system. The description of the *lines* and the *points* is the same as that in Fig. 9b. **d** The enlargement of the bistability region in **c**

strength is varied to hunt different firing patterns. It can be seen that with increasing $g_{syn}$, an inverse period-adding firing sequence can be evidently observed. For the sake of clearness, Fig. 12 only shows the time courses of inverse-adding firing sequence from period $-1$ to 4, where $g_{syn}$ is chosen as 1.1, 1.05, 0.97 and 0.95, respectively. It is noted that the two-coupled system can exhibit "compound bursting", that is, the bursting rhythm consists of two kinds of sub-bursting with different spike amplitudes. For convenience, we refer to the sub-bursting with larger amplitude as sub-bursting 1, and the other as sub-bursting 2. It is seen that both the number of spikes and the width of sub-bursting 1 and 2 are almost equal. Moreover, two cells are in AP synchronization. In other words, when one cell happens to be in the active phase of sub-bursting 1, the other cell just experiences the active phase of sub-bursting 2, and then vice verse. From Fig. 12 it is seen that when $g_{syn} = 1.1$ both sub-bursting 1 and 2 have only one spike in

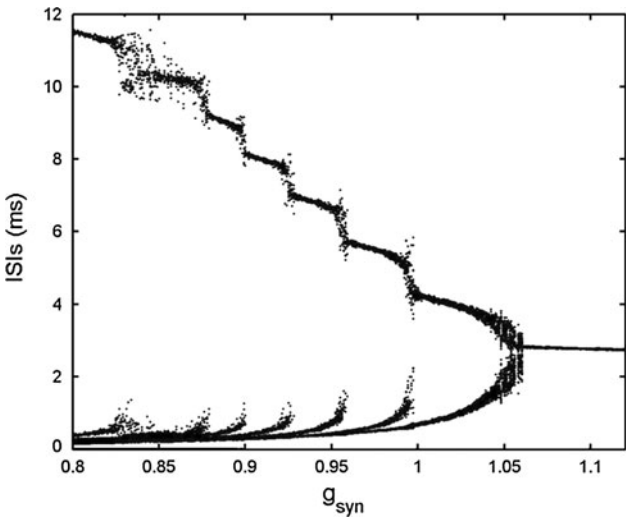


**Fig. 11** Bifurcation *diagram* of ISIs versus the chemical coupling strength $g_{syn}$ in the two chemically coupled cells

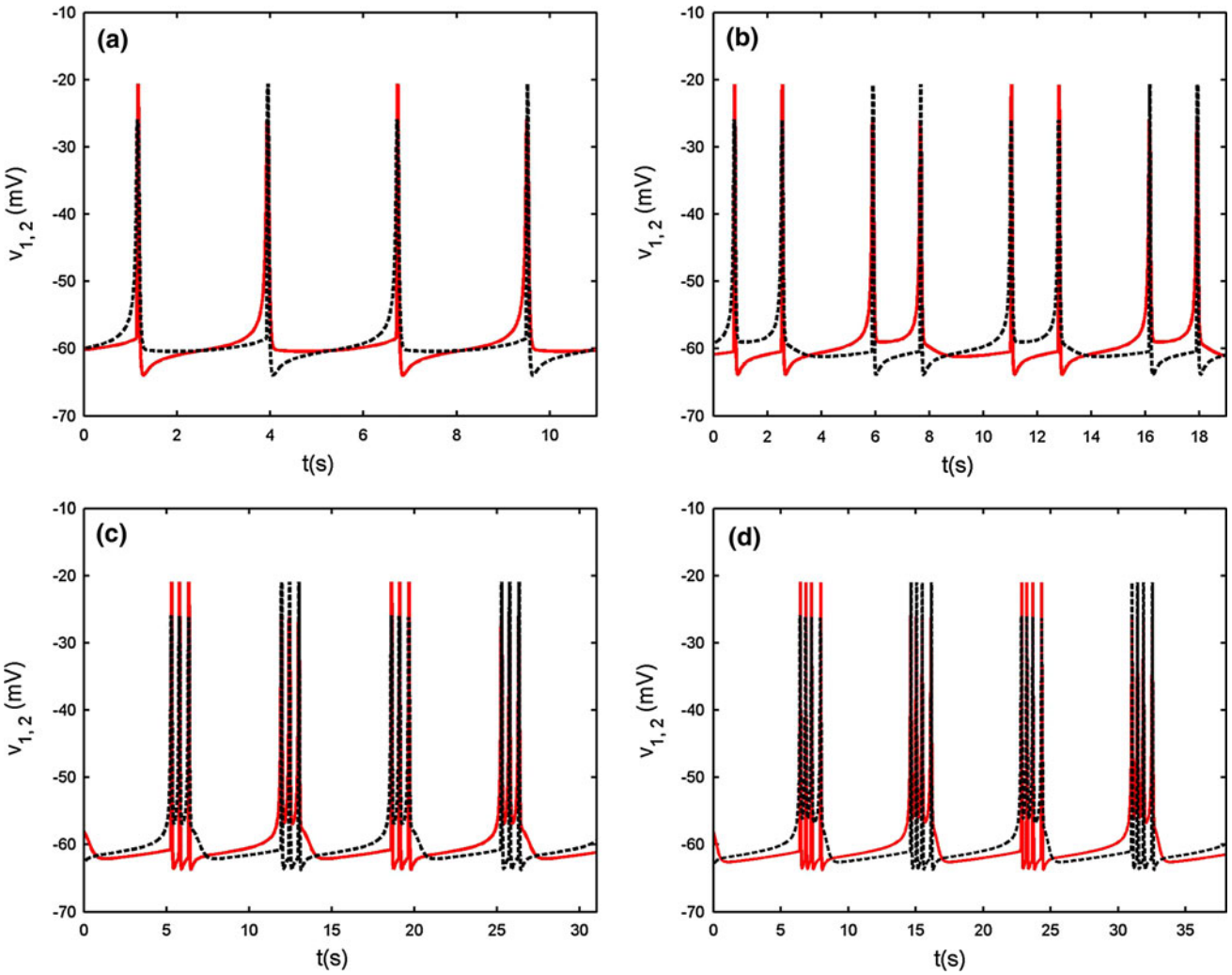


**Fig. 12** Time courses of the membrane potentials of the period-adding firing sequence from period −1 to 4 with $g_{syn} = 1.1$, 1.05, 0.97 and 0.95, respectively. The *red solid lines* and the *black dashed lines* represent the time courses for the variable $v_1$ and $v_2$, respectively. (Color figure online)

a burst. When $g_{syn}$ is decreased to 1.05, 0.97 and 0.95, respectively, the number of spikes in a burst is increased to 2, 3, 4 continuously. This clearly claims the existence of the inverse period-adding sequence.

When the chemical coupling strength is increased to $g_{syn} = 2.4$, the two cells can realize complete bursting synchronization (see Fig. 13a, b). Hence $s_1 = s_2$ holds strictly Fast–slow dynamics analysis can be used to explain the generation mechanism of this type of bursting. The stationary branch is not $Z$ shaped curve, but it has fourfold bifurcations instead. The curve of equilibria of the fast subsystem can be divided into three parts, that is, the upper, middle and lower parts, respectively. The middle part is connected by fold bifurcations F3 and F4, and it is composed of the saddles of the fast subsystem. The upper part is that above the middle part and is composed of foci of the fast subsystem. The remainder is named as the lower part, which is coincident with the $Z$ shaped curve of the single cell before (see Fig. 13c). Therefore, the upper part, the middle part and the lower sub-branches of the lower part have the same meaning as before and are composed of foci, saddle and node, respectively. Here we notice that although the steady states both on the middle part and the middle sub-branch of the lower part are saddles, but their eigenvalues have different characters. The saddle on the middle part has three negative eigenvalues and one positive eigenvalue, while the saddle on the middle sub-branch of the lower part has two negative eigenvalues and two positive ones, respectively. Thus, both of which are double roots. The silent phase of bursting ends with the fold bifurcation F1, and then the trajectory is attracted by the stable foci in the upper part to start bursting. With $s$ increasing, the stable focus in the upper part becomes unstable via the subHopf bifurcation H2 (see Fig. 13d), and these results in the transition to the silent phase of bursting. Thus the coupled system is capable of the "fold/subHopf"

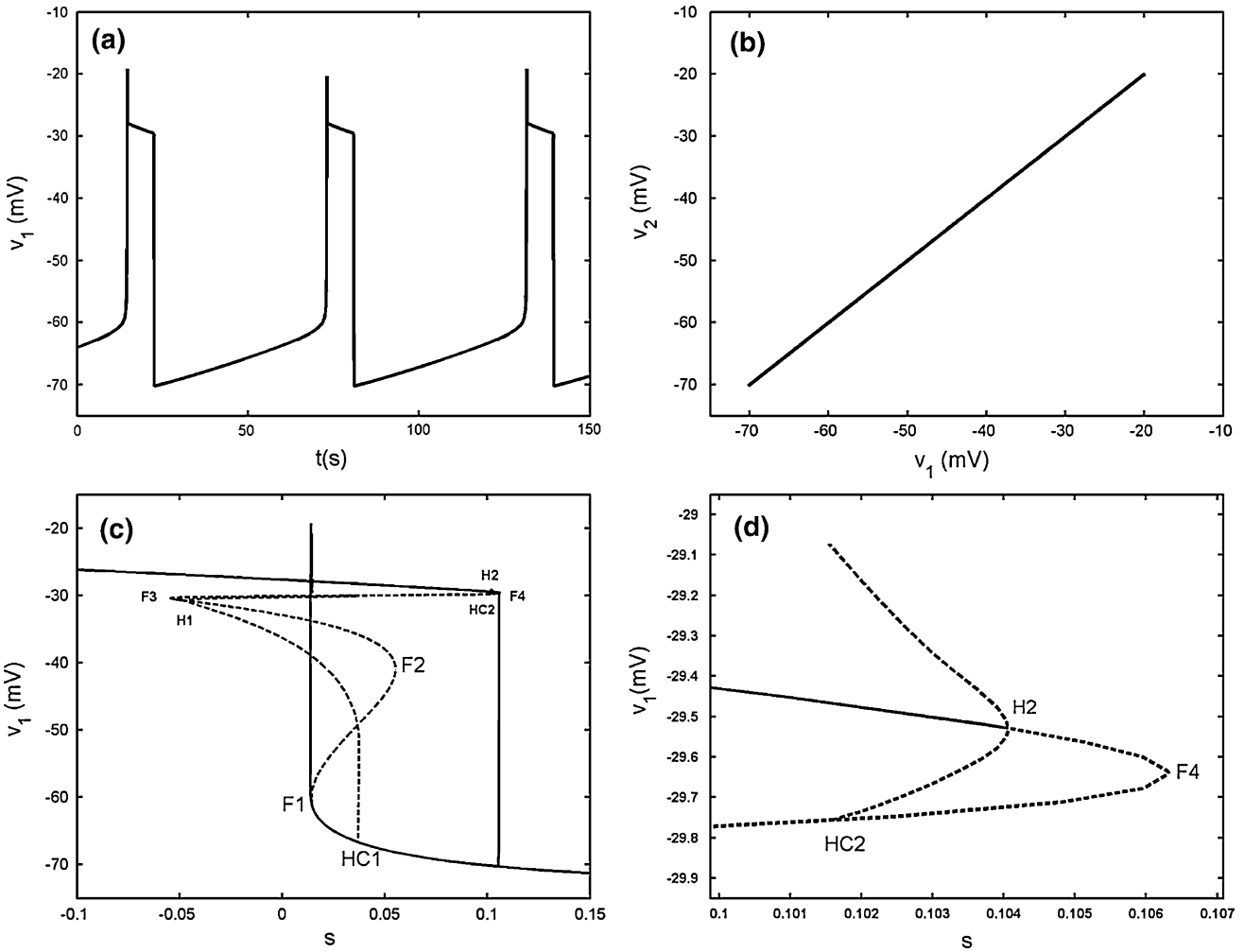


**Fig. 13** Two chemically coupled cells with $g_s = 4$, $g_{syn} = 2.4$. **a** Time series of the variable $v_1$. **b** The projection on ($v_1$, $v_2$) plane. **c** Fast–slow dynamics analysis of the chemically coupled system. The *solid* and *dashed lines* represent the stable and unstable states, respectively. F1–F4 are the fold bifurcations, respectively. H1 and H2 refer to the subHopf bifurcations. HC1 and HC2 refer to the homoclinic bifurcations. **d** The enlargement of the region near the point H2

type of bursting. It is noticed that there exists a subHopf bifurcation H1 in the upper sub-branch of the lower part but it does not influence the shape of bursting pattern.

## Conclusion

In summary, the effects of electrical and chemical coupling on synchronization behaviors of coupled pancreatic $\beta$-cells are investigated by extending the fast–slow dynamics analysis from single cell to the coupled cells. For two electrically coupled cells, when an isolated cell exhibits continuous spiking individually, with the coupling strength increasing, there exists synchronization transition with at least four different synchronous states, including two kinds of bursting synchronization with totally different bifurcation structure of the fast subsystem, and another two synchronous spiking regimes with continuous AP and IP rhythms, respectively. For the model used in this paper, these results explain the role of the electrical coupling in more detail comparing to the previous results. For two chemically coupled cells, two spiking cells can transit to bursting under weak chemical coupling condition. Moreover, an interesting inverse period-adding bursting sequence in the coupled cells is found when the isolated cell exhibits square-wave bursting. In addition, the two coupled cells with proper chemical coupling strength can produce the "fold/subHopf" type of bursting. Our bifurcation analysis is based on the assumption that the slow variables of two cells $s_1 \approx s_2$. Thus $s = s_1 = s_2$ could be taken as the bifurcation parameter. In fact, this assumption is valid mostly except the inverse period-adding bursting sequence occurring in the chemically coupled cells. The latter case is worthy of the further research.

**Acknowledgments** This work was supported by the National Natural Science Foundation of China (No. 11172017).

## Appendix

See Figs. 14 and 15.

The model for a single pancreatic $\beta$-cell is described by the following equations:

$$\tau \frac{dv}{dt} = -I_{Ca}(v) - I_k(v,n) - I_s(v,s) - I_{K(ATP)}(v,p) \quad (7)$$

$$\tau \frac{dn}{dt} = \lambda[n_\infty(v) - n] \quad (8)$$

$$\tau_s \frac{ds}{dt} = s_\infty(v) - s \quad (9)$$

Three variables in this system are: the membrane potential ($v$), the delayed rectifier activation ($n$), and a very slow variable $s$ which has been postulated to be the intracellular $Ca^{2+}$ (Sherman et al. 1988). The $s$ equation is a $Ca^{2+}$-balance equation.

Equation (7) is the current balance equation that determines the membrane potential $v$ and is composed of four ionic currents, which are defined by

$$I_{Ca}(v) = g_{Ca} m_\infty(v)(v - v_{Ca})$$
$$I_K(v,n) = g_K n(v - v_K)$$
$$I_s(v,s) = g_s s(v - v_K)$$
$$I_{K(ATP)}(v,p) = g_{K(ATP)} p(v - v_K)$$

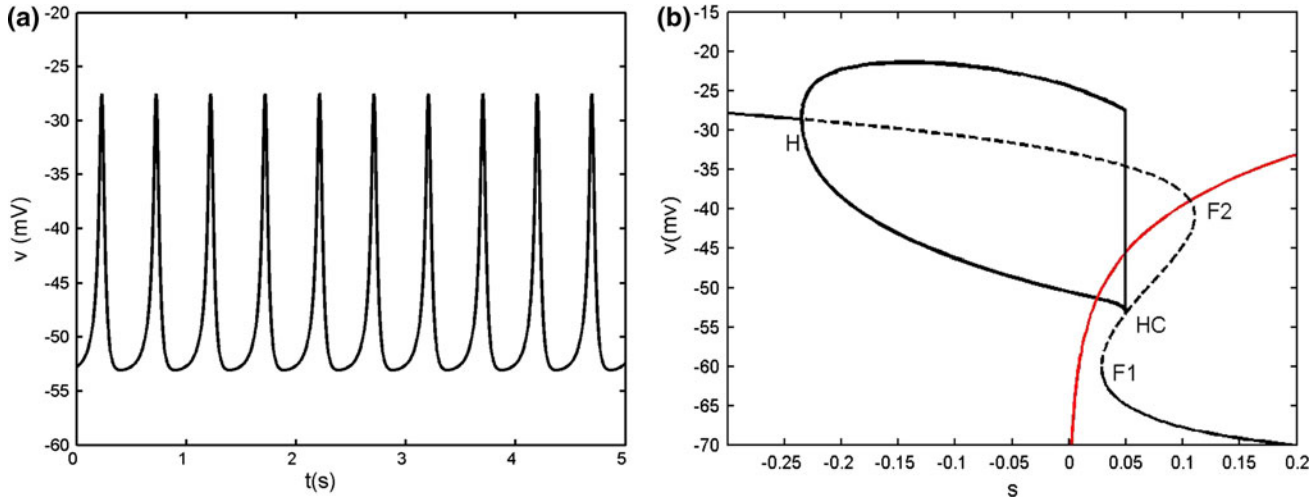


**Fig. 14** **a** Time series of the single model with $g_s = 2$. **b** Bifurcation *diagram* of the fast subsystem of [Eqs. (8), (9)]. H refers to the supHopf bifurcation, F1 and F2 refer to the fold bifurcations, HC refers to the homoclinic bifurcation. The *C* shaped *curve* represents the maximum and minimum values of periodic solutions originated from H. The phase *plot* of the whole system is also superposed on the ($v$, $s$) plane. The *red line* is the $s$-nullcline. (Color figure online)

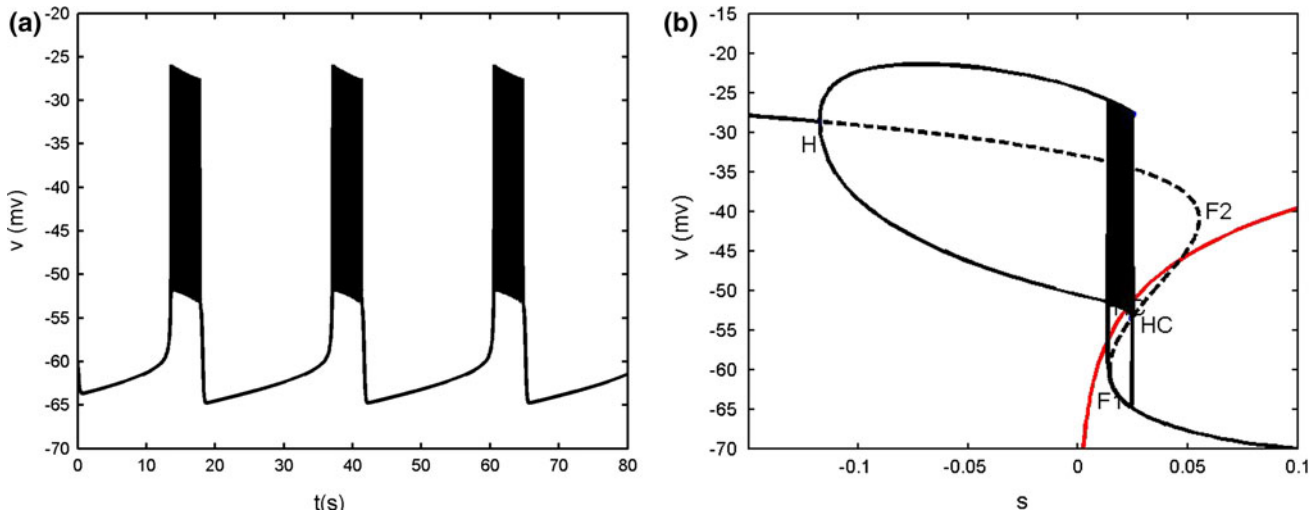


**Fig. 15** **a** Time series of the single model with $g_s = 4$. **b** Bifurcation *diagram* of the fast subsystem. The description of the *lines* and *points* is the same as that in Fig. 14b

with the constant conductance $g_{Ca}$, $g_K$, $g_s$ and $g_{K(ATP)}$ and the reversal potentials $v_{Ca}$, $v_K$ for $Ca^{2+}$ and $K^+$ ions, respectively. $I_{Ca}$ is assumed to respond instantaneously to a change in membrane potential with the steady state function $m_\infty(v)$, while the dynamics for $I_K$ is governed by the gating variable $n$ via Eq. (2), where $\tau$ is the activation time constant for the delayed rectifier $K^+$ channel, and $n_\infty(v)$ is the equilibrium function for the activation variable $n$. In the expression of $I_{K(ATP)}$, $p$ is the fraction of the open K(ATP) channels. The dynamics for $I_s$ is similar to that of $I_K$. But comparing with $\tau$, the time constant $\tau_s$ becomes much bigger.

The equilibrium functions $m_\infty(v)$, $n_\infty(v)$ and $s_\infty(v)$ have the general expression given by $x_\infty(v)$ as follows:

$$x_\infty(v) = [1 + e^{(v_x - v)/\theta_x}]^{-1}, \quad x = m,\ n,\ s$$

Since $\tau_s >> \tau$, $s$ responds on a much slower time scale than $v$ and $n$. Thus Eqs. (7)–(9) construct a system with both slow and fast scales. The fast subsystem is composed of Eqs. (7) and (8), in which the slow variable $s$ is considered as the bifurcation parameter. The trajectory of the whole system is then superimposed on the bifurcation diagram of the fast subsystem to explain the dynamical behavior of the model; this is the fast–slow dynamics analysis (Rinzel 1987).

All the parameters are listed in Table 1. Depending on the value of the parameter $g_s$, the system either undergoes a spiking solution or generates bursting oscillations. Both of which can be explained by using fast–slow dynamics analysis. The details of the two typical cases are explained as follows.

When $g_s = 2$, the single cell gives continuous spiking (see Fig. 14a). The bifurcation diagram of the fast subsystem with respect to the slow variable $s$ is plotted in Fig. 14b. The equilibrium points form a $Z$ shaped curve in ($v$, $s$) plane. The $Z$ shaped curve is made up of the upper, middle and the lower branch. With the increase of $s$, the stable foci on the upper branch become unstable via a supHopf bifurcation H at $s = -0.235$. A branch of stable limit cycle oscillations emerges from the H point, and it terminates at homoclinic bifurcation HC. The middle and lower branches are composed of saddles and stable nodes, respectively. The $s$-nullcline is also superimposed onto the bifurcation diagram. The dynamics of the full system can be understood by using the $Z$ shaped curve and the $s$-nullcline together. It is seen that the $s$-nullcline intersects the periodic branch and the intersection sufficiently deeps into the periodic branch, so that the system produces continuous spiking (Terman 1992).

When $g_s = 4$, the single cell exhibits a typical bursting oscillation (see Fig. 15a). Fast–slow dynamics analysis is illustrated in Fig. 15b. It is noticed that $g_s$ is not involved in the slow subsystem. Hence, it has no effect on the $s$-nullcline. Compared with Fig. 14b, it is seen that the $s$-nullcline still intersects with the periodic branch, and at this time the intersection is near the end of the periodic branch. If the variable $s$ varied very slowly, this would result in continuous spiking. However, $s$ does not vary such slow actually in this case so that the bursting can be produced (Terman 1992). Moreover, for values of $s$ between the left knee of the $Z$ shaped curve and the homoclinic bifurcation, there is bistablility between the stable node state on the lower branch, which corresponds to the silent phase of bursting, and the stable limit cycle oscillation corresponding to the active phase of bursting. The silent phase disappears via the fold bifurcation F1, and the active phase ends with the homoclinic bifurcation HC. Since this type of bursting depends on passing through both fold and homoclinic bifurcations, it is called as "fold/homoclinic" bursting (Perc and Marhl 2003). It is also known as "square-wave" bursting, due to the fact that the active phase spikes rise from a plateau (Rinzel 1987).

## References


Arenas A, Diaz-Guilera A, Kurths J, Moreno Y, Zhou CS (2008) Synchronization in complex networks. Phys Rep 469(3):93–153

Ashcroft FM, Rorsman P (1989) Electrophysiology of the pancreatic $\beta$-cell. Prog Biophys Mol Biol 54:87–143

Bergsten P (2000) Pathophysiology of impaired pulsatile in insulin release. Diabetes Metab Res Rev 16:179–191

Calabrese A, Bosco D, Soria B, Wollheim CB, Herrera PL, Meda P (2000) Junctional communication of pancreatic $\beta$-cells contributes to the control of insulin secretion and glucose tolerance. J Clin Invest 106:235–243

Cunningham BA, Deeney JT, Bliss CR, Corkey BE, Tornheim K (1996) Glucose-induced oscillatory insulin secretion in perifused rat pancreatic and clonal $\beta$-cells (HIT). Am J Physiol 271: 702–710

De Vries G, Sherman A (1998) Diffusively coupled bursters: effects of cell heterogeneity. Bull Math Biol 60:1167–1199

De Vries G, Sherman A (2000) Channel sharing in pancreatic $\beta$-cells revisited: enhancement of emergent bursting by noise. J Theor Biol 207:513–530

Dean PM, Mathews EK (1970) Glucose induced-electrical activity in pancreatic islet cells. J Physiol 210(2):255–264

Eddlestone GT, Goncalves A, Bangham JA, Rojas E (1984) Electrical coupling between cells in islets of Langerhans from mouse. J Memb Biol 77:1–14

Gomez-Gardenes J, Moreno Y, Arenas A (2007) Paths to synchronization on complex networks. Phys Rev Lett 98:034101

Izhikevich EM (2000) Neural excitability, spiking and bursting. Int J Bifurcat Chaos 10:1171–1266

Kennedy RT, Kauri LM, Dahlgren GM, Jung SK (2002) Metabolic oscillations in $\beta$-cells. Diabetes 51(Suppl 1):52–61

Krasimira TA, Zimliki CharlesL, Bertram R, Sherman A (2006) Diffusion of calcium and metabolites in pancreatic islets: killing oscillations with a pitchfork. J Biophys 90:3434–3446

Marek M, Stuchl I (1975) Synchronization in two interacting oscillatory systems. Biophys Chem 3(3):241–248

Meissner HP (1976) Electrophysiological evidence for coupling between $\beta$-cells of pancreatic islets. Nature 262:502–504

Orci L, Malaisse-Lagae F, Amherdt M, Ravazzola M, Weisswange A, Dobbs R, Perrelet A, Unger R (1975) Cell contacts in human islets of Langerhans. J Clin Endocrinol Metab 41:841–844

Perc M, Marhl M (2003) Different types of bursting calcium oscillations in non-excitable cells. Chaos Solitons Fractals 18: 759–773

Perc M, Marhl M (2004a) Local dissipation and coupling properties of cellular oscillators: a case study on calcium oscillations. Bioelectrochemistry 62:1–10

Perc M, Marhl M (2004b) Synchronization of regular and chaotic oscillations: the role of local divergence and the slow passage effect. Int J Bifurcat Chaos 14:2735–2751

Ravier MA, Gilon P, Henquine JC (1999) Oscillations of insulin secretion can be triggered by imposed oscillations of cytoplasmic $Ca^{2+}$ or metabolism in normal mouse islets. Diabetes 48(12):2374–2382

Rinzel J (1987) A formal classification of bursting mechanisms in excitable systems. In: Teramot E, Yamaguti M (eds) Mathematical topics in population biology, morphogenesis and neurosciences, vol 71. Lecture Notes in Biomathematics. Springer, Berlin, pp 267–281

Rorsman P, Berggren PO, Bokvist K, Ericson H, Mohler H, Ostenson CG, Smith PA (1989) Glucose-inhibition of glucagon secretion involves activation of GABAA-receptor chloride channels. Nature 341:233–236

Rubin J, Terman D (2002) Geometric singular perturbation analysis of neuronal dynamics. In: Fiedler B (ed) Handbook of dynamical systems, vol 2. Elsevier, pp 93–146

Salehi A, Qader SS, Grapengiesser E, Hellman B (2005) Inhibition of purinoceptors amplifies glucose-stimulated insulin release with removal of its pulsatility. Diabetes 54:2126–2131

Sherman A (1994) Anti-phase, asymmetric and aperiodic oscillations in excitable cells—I. Coupled bursters. Bull Math Biol 56: 811–835

Sherman A, Rinzel J (1991) Model for synchronization of pancreatic beta-cells by gap junctions. J Biophys 59:547–559

Sherman A, Rinzel J (1992) Rhythmogenic effects of weak electrotonic coupling in neuronal models. Proc Natl Acad Sci USA 89:2471–2474

Sherman A, Rinzel J, Keizer J (1988) Emergence of organized bursting in clusters of pancreatic $\beta$-cells by channel sharing. J Biophys 54:411–425

Sun XJ, Lei JZ, Perc M, Kurths J, Chen GR (2011) Burst synchronization transitions in a neuronal network of subnetworks. Chaos 21:016110

Terman D (1992) The transition from bursting to continuous spiking in excitable models. J Nonlinear Sci 2:135–182

Valdeolmillos M, Gomis A, Sanchez-Andres JV (1996) In vivo synchronous membrane potential oscillations in mouse pancreatic $\beta$-cells: lack of co-ordination between islets. J Physiol 493:9–18

Volman V, Perc M, Bazhenov M (2011) Gap junctions and epileptic seizures—two sides of the same coin? PLoS One 6:e20572

Wang R, Jiao X (2006) A stochastic nonlinear evolution model and neural coding on neuronal population possessing variable coupling intensity in spontaneous behavior. Neurocomputing 69(7–9):778–785

Wang R, Zhang Z (2003) Nonlinear stochastic models of neurons activities. Neurocomputing 51:401–411

Wang QY, Chen GR, Perc M (2011) Synchronous bursts on scale-free neuronal networks with attractive and repulsive coupling. PLoS One 6(1):e15851

Zhang Q, Galvanovskis J, Abdulkader F, Partridge CJ, Göpel S, Eliasson L, Rorsman P (2008) Cell coupling in mouse pancreatic $\beta$-cells measured in intact islets of Langerhans. Phil Trans R Soc A 366:3503–3523

Zhang X, Wang R, Zhang Z, Qu J, Cao J, Jiao X (2010) Dynamic phase synchronization characteristics of variable high-order coupled neuronal oscillator population. Neurocomputing 73:2665–2670